The effect of spherical aberration on temperature distribution inside glass by irradiation of a high repetition rate femtosecond pulse laser*

Dai Ye(戴 晔)†, Yu Guang-Jun(余光军), Wu Guo-Rui(武国睿),
Ma Hong-Liang(马洪良), Yan Xiao-Na(阎晓娜), and Ma Guo-Hong(马国宏)

Department of Physics, Shanghai University, Shanghai 200444, *China*

(Received 19 July 2011; revised manuscript received 15 August 2011)

In this paper, we study the effect of spherical aberrations on the light intensity and the temperature distribution in the focal region in a 250-kHz femtosecond laser irradiated Ag^{+}-doped borosilicate glass. When a focused beam goes through an interface between air and glass, spherical aberration will result in the separation of the focal point and then cause a clear change of the light intensity distribution along the incident direction. That phenomenon will further influence the longitudinal cross-section temperature distribution in glass. Here we use Ag nanoparticle formation as a marker for establishing temperature distribution and we find that the formation of nanoparticle shows a strong dependence on the temperature field and the detailed precipitation process is also discussed.

Keywords: femtosecond laser, glass, spherical aberration, heat accumulation effect

PACS: 52.38.Mf, 42.15.Fr, 78.20.nb, 82.60.Nh **DOI:** 10.1088/1674-1056/21/2/025201

1. Introduction

The interaction of femtosecond (fs) pulse laser with transparent materials is a fast developing research field of optics. It has shown many novel nonlinear phenomena resulting from the simultaneous multiphoton absorption or ionization in the photon-excited region due to ultrashort interaction time and ultrahigh power density of fs pulse.[1−8] Due to the fact that this kind of subwavelength photon excitation mechanism can strictly confine the structure change region, one can achieve both space-selective and high-precision micromachining inside the bulk materials. In the past few years, a variety of functional microstructures have been produced by this method and then applied to the fabrication of photonics devices, such as optical waveguides,[1,2] optical storages,[3−5] micro/nano gratings,[6−8] and so on. Generally, the impact of light-heat effect in fs pulse laser micromachining is eliminated as far as possible in order to achieve a fine structure. However, recent studies show that heat accumulation effect will play an important role in promoting the evolution of the microstructure in the case that the transparent material is irradiated by a high repetition rate fs pulse laser. When the interval time between two pulses is obviously shorter than that time for the heat diffusing out of the focal volume, the temperature of the focal volume will increase drastically due to the continuous energy deposition within many pulses irradiating. As a result, a series of heat-related structural changes occurs.[9−11]

In previous reports, a few groups have carried out some valuable explorations on the relationship between structure modification and heat accumulation effect.[12−14] Schaffer *et al.*[12] proposed that a heat accumulation would cause structure expansion in the focal point when an 82-MHz fs laser oscillator was used to machine bulk glass. Eaton *et al.*[13] also analysed a transition from thermal diffusion to heat accumulation using an fs laser system with repetition rate varying from 0.2 MHz to 5 MHz. Recently, Shimizu *et al.*[14] systematically studied the temperature distribution and modification mechanism inside a glass after a 250-kHz fs pulse laser irradiation. The above studies greatly improved our understanding of the mechanism of fs laser induced heat accumulation effect. However, most of these temperature distribution models are based on an approach that propagation and focus-

*Project supported by the National Natural Science Foundation of China (Grant No. 60908007) and the Shanghai Leading Academic Discipline Project, China (Grant No. S30105).

†Corresponding author. E-mail: yedai@shu.edu.cn

© 2012 Chinese Physical Society and IOP Publishing Ltd

ing of fs laser follow the geometric optical laws without considering the influence of spherical aberration. In fact, spherical aberration certainly arises when an incident light is focused through an interface between two media with different dielectric properties, e.g. air and glass.[15−17] Therefore, the light intensity along the optical axis will not be confined to a central focus but into a line distribution, which means that the size and the shape of heat-modified region have changed. In order to obtain an optimized model, it is necessary to take into consideration the effect of spherical aberration on the temperature distribution in the heat-modified region.

In this paper, we first propose a temperature model based on both spherical aberration effect and heat diffusion equation to simulate the temperature distribution in the longitudinal cross section of the heat-modified region. In the experiments, we perform the precipitation of silver nanoparticles inside a bulk glass using a 250-kHz fs pulse laser. By comparing the nanoparticle precipitation area with the simulated temperature distribution, the effect of spherical aberration on heat-modified region is further discussed. We think that this technique could provide an anisotropic heat source to modify transparent materials.

2. Experiment

In this study, a glass sample with $10Na_2O$–$6K_2O$–$3BaO$–$11B_2O_3$–$70SiO_2$–$0.05Ag_2O$ (mol%) was prepared by the conventional melt-quenching method. The detailed fabrication process was described elsewhere.[18] A regenerative amplified Ti: sapphire laser system (Coherent, RegA 9000) emits 800 nm, 150 fs and 250-kHz pulses and then these pulses were focused to different focal depths in the interior of the glass through an optical microscope (Olympus, BX51) and a computer-controlled XYZ stage (Prior, ProScan). The transmission loss of pulse energy was about 20% when a beam with a diameter of 3 mm was focused by an objective (20x, NA=0.45). The exposure time of the incident fs laser was controlled by an electronic shutter. All the irradiation was carried out at room temperature.

3. Simulation of temperature distribution

3.1. Spherical aberration

As shown in Fig. 1, a laser beam focused by the microscope objective lens first propagates through an air–glass interface and then enters into the glass along the $+z$ axis. Suppose that if glass does not exist and spherical aberration is ignored, then this laser beam will be focused to a point O_1 after having passed through the microscope objective lens and the focal depth is d, as illustrated by the dotted lines. However once a converging spherical wave is incident on the air–glass interface n_1/n_2, the phase of the transmitted field will be changed and the light goes to a new focal point O_2 because of refractive index mismatch. Furthermore, the curvature radius of the lens is very difficult to be consistent due to the fabrication precision. Therefore, all the light will be discretely focused to many new focal points from O_1 to O_2 along the optical axis instead of converging to a central focus. This phenomenon of separation of the focal point implies the emergence of spherical aberration.

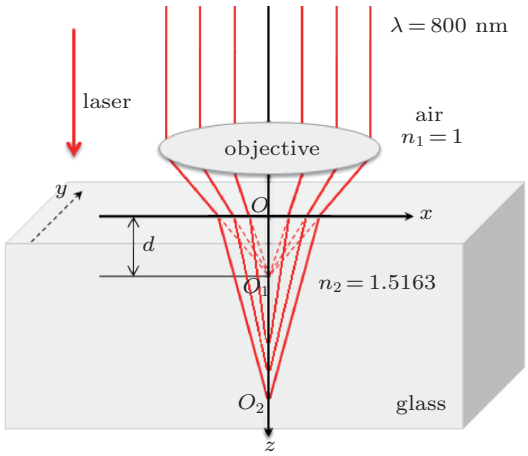


Fig. 1. (colour online) An illustration of spherical aberration effect from air to glass.

We calculated the light intensity distribution near the focus of objective in the presence of the refractive index mismatch. For the situation illustrated in Fig. 1, the resulting electric field distribution in glass is given by[17,19,20]

$$I = \int_0^{\alpha} (\cos\phi_1)^{1/2}(\sin\phi_1)\exp[-\mathrm{i}\,k_0 d(n_1\cos\phi_1 - n_2\cos\phi_2)] \times (\tau_\mathrm{s} + \tau_\mathrm{p}\cos\phi_2) \mathrm{J}_0[k_1(x^2+y^2)^{1/2}\sin\phi_1]\exp(\mathrm{i}\,k_2 z\cos\phi_2)\,\mathrm{d}\phi_1, \quad (1)$$

where α is the half angle of the light convergence cone, $k_0 = 2\pi/\lambda$ is the wave number in vacuum, J_0 is the Bessel function of the first kind and zeroth order and d is the depth of the geometrical focal point from the interface to glass (see Fig. 1). In addition, ϕ_1 and ϕ_2 are the angles of the beam convergence in the first and second media respectively. The coefficients τ_s and τ_p are the Fresnel transmission coefficients for s and p polarizations and are functions of ϕ_1 and ϕ_2, expressed as

$$\tau_s = \frac{2\sin\phi_2\cos\phi_1}{\sin(\phi_1+\phi_2)}, \tag{2}$$

and

$$\tau_p = \frac{2\sin\phi_2\cos\phi_1}{\sin(\phi_1+\phi_2)\cos(\phi_1-\phi_2)}. \tag{3}$$

3.2. Solution to heat diffusion equation

In this case, the Cartesian coordinates are fixed in space and are static with respect to the beam. The origin is set on the surface (x–y plane) and is directly underneath the beam centre. The $+z$ axis spreads into the bulk glass. Under these conditions, the differential equation describing heat diffusion is given by[13]

$$\rho C_p \frac{\partial T}{\partial t} = \kappa\left(\frac{\partial^2 T}{\partial x^2} + \frac{\partial^2 T}{\partial y^2} + \frac{\partial^2 T}{\partial z^2}\right) - \frac{\partial I}{\partial z}, \tag{4}$$

where ρ is the glass density, C_p is glass heat capacity, κ is thermal conductivity of glass, I is the laser intensity and T is the glass temperature. Spatial and temporal coordinates are x, y, z and t respectively. As the glass composition used in our experiment is exactly similar to the BK7 glass of Schott, we refer to its data sheet of ρ [2.53 g/cm^3], C_p [0.858 J/(g·k)], κ [0.006 cm^2/s] for this calculation.[21] Meanwhile, the very close correspondence between the numerical data and the experimental data was obtained for a 50% absorption of laser energy by the glass, which is well consistent with the reported result from Ref. [13]. Although the absorption rate would change a little with the increase of light intensity and glass temperature, we still assume that it is temperature-independent during the irradiation process for the purpose of simplifying the temperature model. Using Eqs. (1)–(4), we calculate $\Delta T_1(x, y, z, t)$, the temperature variation after irradiation of one fs pulse. Due to the continuous injection and diffusion of laser energy, the temperature distribution after N pulse irradiations can be written as

$$\begin{aligned} &T(x, y, z, N\Delta t_L + t) \\ &= T_a + \sum_{n=0}^{N-1} \Delta T_1(x, y, z, n\Delta t_L + t), \end{aligned} \tag{5}$$

where T_a is the ambient temperature, N is the number of fs pulses, Δt_L is the time interval between two pulses and t is heat diffusion time after last pulse.

4. Results and discussion

The temperature distribution of laser-affect zone is determined by a number of irradiation parameters, such as laser power, exposure time, pulse repetition rate, room temperature, etc. Shimizu *et al.*[14] have analysed the influence of these parameters on an x–y plane temperature distribution in a heat-modified region inside a soda lime glass. Here, we focused mainly on a longitudinal cross-section temperature distribution through introducing a spherical aberration effect, which varies dramatically with adjusting focal depth.

Figures 2(a)–2(c) show the simulated temperature distributions in the x–z plane at different focal depths after irradiation of 0.1 s. The incident power was 880 mW and the numerical aperture (N.A.) of microscope objective lens was 0.45. Figure 2(d) also shows the changes of temperature distribution along the z axis through comparing three temperature curves with respective focal depths at 100, 200, and 300 μm. In these simulations, there are two aspects to highlight the effect of spherical aberration on temperature distribution. First, the longitudinal length of the temperature field becomes longer as a result of separation of focal point. Second, under the same irradiation time, the central maximum of temperature distribution gradually decreased with focal depth increasing. It is because the expansion of exposure area decentralizes the incident laser energy. For example, the lengths of the heat modified region with a temperature over 600 °C are respectively 35, 41, and 51 μm when the focal depths are correspondingly at 100, 200, and 300 μm respectively. Consequently, the spherical aberration effect will become more and more remarkable through increasing the focal depth. In other words, it has significantly affected the temperature distribution and subsequently the size and shape of heat-modified region.

In order to better understand the spatial-temporal evolution of temperature distribution in the heat modified region and examine whether the temperature model is reasonable, we used a 250-kHz, 150-fs and 800-nm fs pulse laser to achieve a one-step precipitation of silver nanoparticles without annealing. Figure 3(a) shows a group of top-view micrographs of

the induced structures in Ag-doped glass after various exposure times. The incident power was about 880 mW and the focal depth was 300 μm beneath the surface of the glass. A multilayer ring-shaped structure was generated around the focal centre and the size of this structure obviously increased with exposure time increasing. Since the heat modification mechanisms are not the same in different temperature ranges, the entire structure should be divided into photon-excited area, heat-melted area and heat deformation area.

Figure 3(b) shows their side-view micrographs. There formed an olive-shaped structure with its longitudinal axis along the z direction. Its cross section was substantially similar to the shape of the outmost isotherm in Fig. 2(c), so the experimental results accord with the simulated temperature distributions. Besides, a yellow colour appeared in this structure, which was due to the surface plasmon resonance absorption of the precipitated silver nanoparticles according to our proceeding studies.[18] Furthermore, we also found that the position of silver nanoparticles varied with exposure time increasing. This phenomenon will be discussed in detail in the following context.

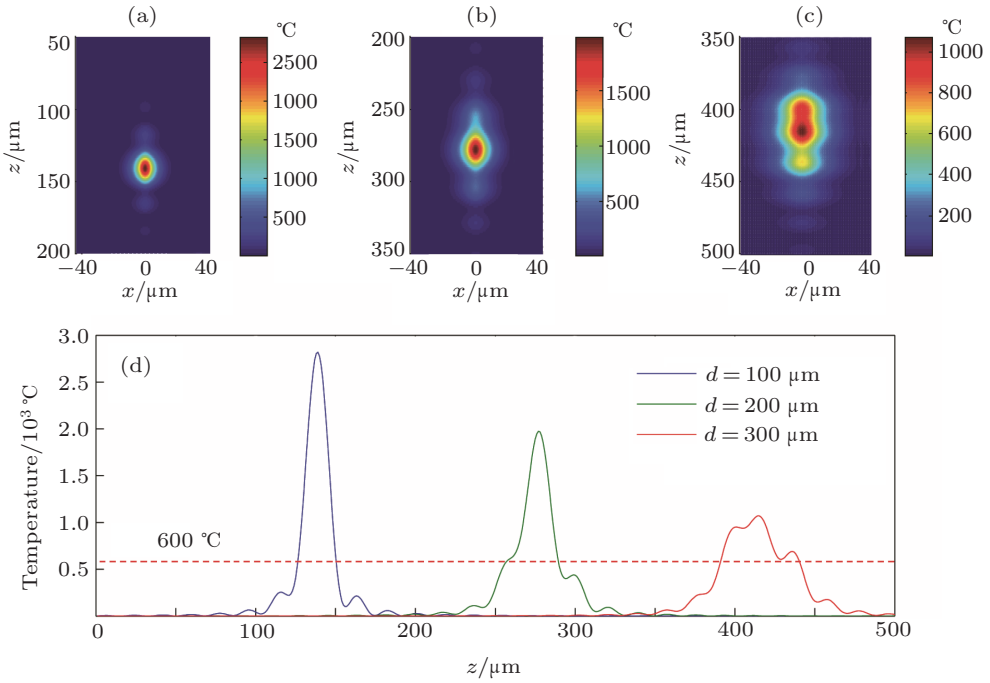


Fig. 2. (colour online) The temperature distributions in the x–z plane (a)–(c) and the z-axis temperature distribution (d) after 0.1 s by a high repetition rate fs pulse laser at different focal depths (d = 100, 200, 300 μm). In the calculations, P = 880 mW and NA=0.45.

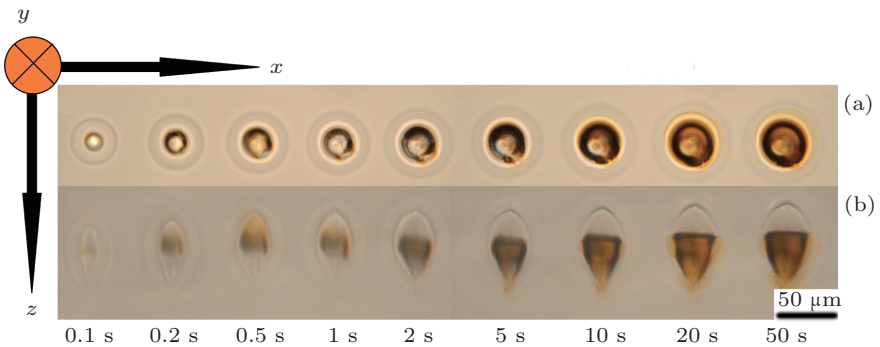


Fig. 3. (colour online) The top-view micrographs (a) and the side-view ones (b) of the induced structures. The exposure time increased from 0.1 s to 50 s.

Here we first explain the reasons for the formation of silver nanoparticles. When an fs pulse laser was focused into the glass, a mass of free electrons were generated through multi-photon ionization and then they combined with Ag ions to form Ag atoms. This process resulted in a lot of reduced Ag atoms occurring in the focal volume. It was known that the mobility of Ag atoms inside glass network is rather inefficient at room temperature, but they would be accelerated dramatically as soon as the glass temperature is high enough.[22,23] In this experiment, the continuous irradiation of the high repetition rate fs pulse laser brought into a high temperature gradient field, thus these reduced Ag atoms might aggregate into nanoparticles and carry on growing according to Ostwald ripening process.[23] Meanwhile, the separations of the focal point also caused an asymmetric temperature distribution. In Figs. 4(a) and 4(b), the cross-section structure was compared with the simulated temperature distribution in the heat-modified region, where the temperatures at A and B were obvious higher than the lower half (C). Therefore the precipitation area of silver nanoparticles gradually spread from the middle part to the upper half of the olive-shaped structure when the exposure time increased from 0.1 s to 0.5 s. Figure 4(c) shows the effect of spherical aberration on the simulated temperature distribution along the z axis. Obviously, the temperature discrepancy between B and C became larger and larger with the extension of exposure time. In the corresponding experiments, we also found that the yellow colour in the upper half of the olive-shaped structure faded away and the silver nanoparticles gradually precipitated into the lower half.

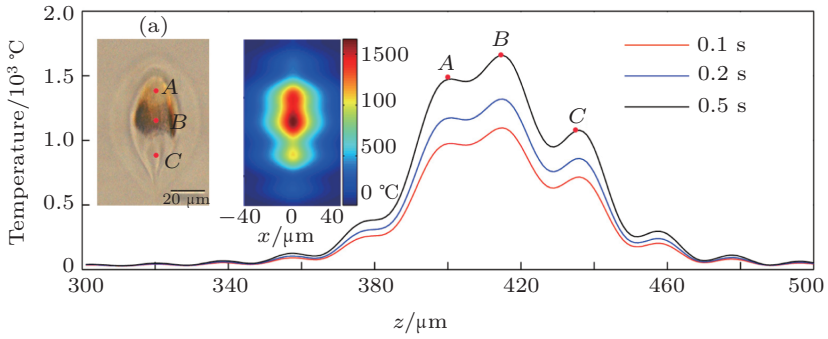


Fig. 4. (colour online) (a) Side-view micrographs and (b) the calculated temperature distributions in the x–z plane with the exposure time of 0.5 s. (c) The calculated z-axis temperature distribution with consideration of the spherical aberration at a focal depth of 300 μm.

The mechanism of this transformation can be explained as follows. With the arrival of successive pulses, the temperature around the prime focal point (B) continuously increased to the extent of the glass melting into the liquid state and accordingly these silver nanoparticles were heated to decompose. Therefore, we have reasons to believe that these Ag atoms could continue to immigrate and diffuse under the force of the temperature gradient field. Once the temperature in the lower half was suited for the growth of silver nanoparticles, those Ag atoms would gather there again to form new nanoparticles. According to the aforementioned analysis, we think that the temperature discrepancy between the lower half and the upper half in the olive-shaped structure should be the main reason why the position of silver nanoparticles varied.

However, in the case that the focal depth was 50 μm beneath the surface of the glass, the effect of spherical aberration on the temperature distribution was relatively small and the formed silver nanoparticles only precipitated into the lower half of the laser modified region.[24] This result may be because the focal depth is inadequate so that separation of focal point caused by spherical aberration is not obvious. The same structure also can be observed in this experiment after the silver precipitation area has fully concentrated in the lower half. After a long period of fs pulse laser irradiation, there gradually formed a sharp interface in the middle of the olive-shape structure. We estimate that it is because there reached heat equilibrium on this interface between these two parts. Besides, our recent study also showed that the as-precipitated silver nanoparticles in the irradiated centre would gradually diffuse to the outside with a continuous irradiation.[24] For example, the tempera-

ture in the centre nearly exceeded 1500 °C after 0.5-s irradiation, at such a high temperature silver nanoparticles could not precipitate there, whereas in Fig. 4 we still observed the obvious yellow in the middle part of the olive-shape structure (B point), therefore these precipitated silver nanoparticles must be in the periphery of the ring-shape structure instead of the central area. This phenomenon is closely dependent on the temperature distribution in the x–y plane, so next, we plan to build a three-dimensional temperature model to study the dynamic process of precipitation and diffusion of silver nanoparticles.

5. Conclusion

We studied the effect of spherical aberration on the temperature distribution in glass by irradiation of a high repetition rate fs pulse laser. The results indicate that the separation of focal point caused by the spherical aberration could significantly influence the temperature distribution in the longitudinal cross section of the heat-modified region, which further affects the precipitation position of silver nanoparticles originating from fs laser driven heat-chemical effect. We consider that spherical aberration is an important factor in fs pulse laser micromachining transparent materials especially when the focal depth goes deep. The results in this study are very helpful for directly writing optical waveguides by using a high repetition rate fs pulse laser.

Acknowledgments

The authors are grateful to Dr. Song Juan of Jiangsu University and Dr. Luo Fang-Fang of Shanghai Institute of Optics and Fine Mechanics for their helpful suggestions.

References

[1] Davis K M, Miura K, Sugimoto N and Hirao K 1996 *Opt. Lett.* **21** 1729
[2] Yang W J, Kazansky P G and Svirko Y P 2008 *Nat. Photon.* **2** 99
[3] Glezer E N, Milosavljevic M, Huang L, Finlay R J, Her T H, Callan J P and Mazur E 1996 *Opt. Lett.* **21** 2023
[4] Qiu J, Miura K, Suzuki T, Mitsuyu T and Hirao K 1999 *Appl. Phys. Lett.* **74** 10
[5] Shimotsuma Y, Sakakura M, Kazansky P G, Beresna M, Qiu J, Miura K and Hirao K 2010 *Adv. Mater.* **22** 4039
[6] Shimotsuma Y, Kazansky P G, Qiu J and Hirao K 2003 *Phys. Rev. Lett.* **91** 247405
[7] Zhao Q Z, Malzer S and Wang L J 2007 *Opt. Lett.* **32** 1932
[8] Xiong P X, Jia X, Jia T Q, Deng L, Feng D H, Sun Z R and Xu Z Z 2010 *Acta Phys. Sin.* **59** 311 (in Chinese)
[9] Dai Y, Ma H, Lu B, Yu B, Zhu B and Qiu J 2008 *Opt. Express* **16** 3912
[10] Kanehira S, Miura K and Hirao K 2008 *Appl. Phys. Lett.* **93** 023112
[11] Luo F F, Qian B, Lin G, Xu J, Liao Y, Song J, Sun H, Zhu B, Qiu J R, Zhao Q Z and Xu Z Z 2010 *Opt. Express* **18** 6262
[12] Schaffer C B, Brodeur A, García J F and Mazur E 2001 *Opt. Lett.* **26** 93
[13] Eaton S M, Zhang H, Herman P R, Yoshino F, Shah L, Bovatsek J and Arai A Y 2005 *Opt. Express* **13** 4708
[14] Shimizu M, Sakakura M, Ohnishi M, Shimotsuma Y, Nakaya T, Miura K and Hirao K 2010 *J. Appl. Phys.* **108** 073533
[15] Luo F F, Song J, Hu X, Sun H, Lin G, Pan H, Cheng Y, Liu L, Qiu J R, Zhao Q Z and Xu Z Z 2011 *Opt. Lett.* **36** 2125
[16] Sun Q, Jiang H, Liu Y, Zhou Y, Yang H and Gong Q 2005 *J. Opt.* A **7** 655
[17] Marcinkevičius A, Mizeikis V, Juodkazis S, Matsuo S, Misawa H 2003 *Appl. Phys.* A **76** 257
[18] Dai Y and Qiu J R 2009 *Chin. Phys.* B **18** 2858
[19] Dogariu A C and Rajagopalan R 2000 *Langmuir* **16** 2770
[20] Song J, Wang X, Hu X, Dai Y, Qiu J, Cheng Y and Xu Z 2008 *Appl. Phys. Lett.* **92** 092904
[21] N-BK7 glass data sheet from Schott
[22] Sun H Y, Luo F F, He F, Liao Y and Xu J 2010 *Chin. Phys.* B **19** 054210
[23] Qiu J, Shirai M, Nakaya T, Si J, Jiang X, Zhu C and Hirao K 2002 *Appl. Phys. Lett.* **81** 3040
[24] Dai Y, Yu G, He M, Ma H, Yan X and Ma G 2011 *Appl. Phys.* B **103** 663